

УДК 537.635
PACS 81.05.ue, 76.30.Pk

Магнитный отклик треугольного графона

К. Б. Циберкин^a, М. Гажи^b

^a Пермский государственный национальный исследовательский университет
614990, Пермь, ул. Букирева, д. 15
email: kbtsiberkin@psu.ru

^b Lincoln College, Оксфордский университет, ул. Турл, OX1 3DR, Оксфорд, Великобритания
email: martin.gazi9@gmail.com

В работе рассматривается графон с треугольной структурой – слой графена, функционализированный водородом с одной стороны таким образом, что атомы водорода связаны только с одной из двух графеновых подрешеток. Его магнитные свойства описываются эффективным гамильтонианом Гейзенберга; в исследуемой системе реализуется ферромагнитное упорядочение спинов неспаренных электронов свободных атомов углерода. Вычислена функция отклика на внешнее магнитное поле в приближении спиновых волн и пределе нулевой температуры. Изучен отклик графона на импульс высокочастотного магнитного поля заданной длительности, поле ориентировано в плоскости решётки. Ввиду неприменимости изотропного приближения для спиновых волн отклик намагниченности найден путём численного интегрирования свёртки функции отклика и Фурье-образа поля. Найдено, что в системе возможны резонансы на частотах, соответствующих верхней границе диапазона разрешённых энергий спиновых волн либо седловой точке на поверхности энергий спиновых волн в пространстве импульсов. Оценки характерных частот показывают, что для изучения свойств материала и измерения обменной энергии необходимо использовать технику спектроскопии в терагерцевом или дальнем ИК-диапазоне.

Ключевые слова: графон; отклик намагниченности; спиновые волны

Поступила в редакцию 31.07.2018; принята к опубликованию 25.08.2018

Magnetic response of triangular graphene

К. Tsiberkin^a, M. Gaži^b

^a Perm State University, Bukireva St. 15, 614990, Perm
email: kbtsiberkin@psu.ru

^b Lincoln College, University of Oxford, Turl Street, OX1 3DR, Oxford, UK
email: martin.gazi9@gmail.com

We consider triangular graphene structure – a semi-hydrogenated layer of graphene with hydrogen atoms bonded to one of its sub-lattices only. The response function of graphene to an external magnetic field is evaluated in general using the Heisenberg Hamiltonian model of the structure with exchange energy coefficient J_0 of unknown value (negative due to ferromagnetic behaviour of triangular graphene). The spin wave approach in the limit of near zero temperature is used for the description of the magnetisation. A specific case when the graphene is exposed to a magnetic pulse with a given carrier frequency is examined in greater depth. To obtain the magnetization response, integration over both the frequency space and momentum space is necessary. Due to inapplicability of the isotropic approximation for the given geometry of graphene, integration over momentum space is performed numerically. The calculations show that the resonance of the system occurs at frequencies which correspond to the upper limit of the spin wave energy band and the saddle points of the energy surface. Using these results, further experimental investigation based on THz or far-

infrared spectroscopy can be performed, which can determine the as-yet-unknown exchange energy coefficient J_0 . The coefficient can in turn provide an estimate of a temperature range for which the spin wave approach utilised in our investigation is valid.

Keywords: graphene; magnetization response; spin waves

Received 31.07.2018; accepted 25.08.2018

doi: 10.17072/1994-3598-2018-3-65-72

1. Introduction

Over the last decades, graphene has gained increasing attention due to its two-dimensional planar structure, band crossing at the Dirac points, two sub-lattice semi metallic conduction and hence its possible use in nanoelectronics [1–5]. Graphene however does not exhibit strong magnetic properties, but only weak anti-ferromagnetic order [6, 7]. Several methods such as functionalization of graphene by chemisorptions of atomic hydrogen have been proposed to tune electronic properties and induce magnetic behaviour [8–11]. For this purpose however, only partial hydrogenation proves useful as fully hydrogenated graphene (graphane) does not have a strong magnetic response either [12, 13].

In our investigation, we focus on triangular graphene structure (see Fig. 1, [14]). Triangular graphene is a semi-hydrogenated graphene sheet with all hydrogen atoms bonded only to carbons in one sub-lattice of graphene (key characteristic of the trigonal structure) with all hydrogen atoms on one side [12]. When we refer to graphene, we mean the triangular form, unless stated otherwise. Semi-hydrogenation breaks the delocalized π -bonding present in graphene. As a consequence the p -electrons in the un-

hydrogenated carbon atoms are unpaired and localised, allowing for isotropic exchange interactions. According to the works of Zhou et al, computer simulations based on spin-polarized density functional theory suggest that these interactions result in ferromagnetic properties of graphene [12]. Moreover it also possesses an energy gap, making it an attractive material for use in nano-electronics [7, 12–15].

Possible uses of graphene largely depend on its thermal stability as uncontrollable changes to its structure by hydrogen hopping to neighbouring carbon atoms may significantly alter its conducting and magnetic properties [14]. Several authors including Podlivaev and Openov report high instability of triangular graphene (with characteristic time of disordering of the structure shorter than 1 ns at liquid-nitrogen temperatures) [13, 16], and its evolution via hydrogen hopping into more stable rectangular graphene (see Fig.2, [14]) which exhibits anti-ferromagnetic behaviour [14]. The study of Hemmatiyan et al. however suggests a method of stabilising triangular graphene using hexagonal boron-nitride (h-BN) [7]. Substrate creates dipole moments for each nitrogen site that break the equivalency of two carbon atoms in two different graphene sub-lattices, hence suppressing the hydrogen migration.

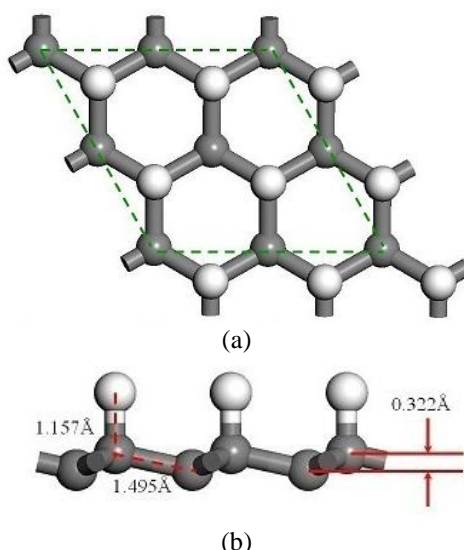


Fig. 1. Geometric structure of triangular graphene. (a) Top view with carbon atoms shown grey and hydrogen atoms shown white, (b) side view shows C-C and C-H bond lengths and distances

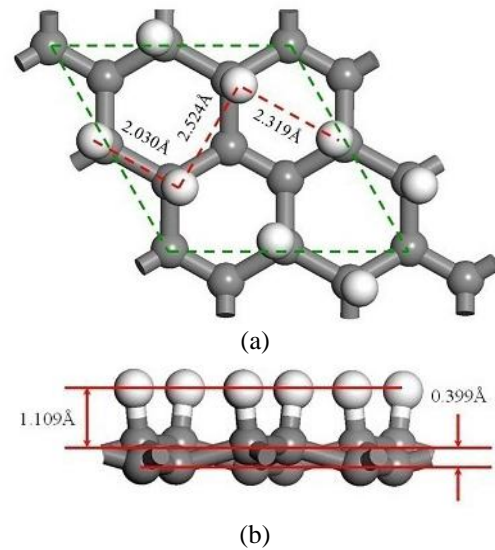


Fig. 2. Geometric structure of rectangular graphene. (a) Top view with carbon atoms shown grey and hydrogen atoms shown white, (b) side view shows C-H bond length and sub-lattice separation

2. System response function

Throughout our analysis, we will be using Planck units and hence \hbar normalizes to 1. The triangular graphene layer is assumed to be effectively a 2D sheet oriented in the x - y plane. We consider the limit of 0 K temperature.

In the presence of localised spins S of the p-electrons of un-hydrogenated carbons at lattice sites i and j ($i \neq j$), the tight-binding free hopping Hamiltonian of the structure

$$\mathcal{H}_0 = -t' \sum_{\langle i,j \rangle} (a_i^\dagger a_j + a_j^\dagger a_i), \quad (2.1)$$

which allows for electrons to hop (quantum tunnel) between sites i and j on the same graphene sub-lattice (different sub-lattice jump not possible due to C-H bonds) is effectively represented by the spin exchange Heisenberg Hamiltonian

$$\mathcal{H}_1 = \sum_{\langle i,j \rangle} J_{ij} S_i \cdot S_j, \quad (2.2)$$

In the equations above, a_i^\dagger (a_i) creates (annihilates) an electron on site i , and t' is the next nearest-neighbour hopping energy (value not well known, calculations show value $t' \approx 0.1$ eV) [1, 17]. Because of the isotropy of the triangular graphene structure J_{ij} is constant J_0 , which is negative due to ferromagnetic behaviour [4, 12].

Using spin raising and lowering operators

$$S^\pm = S^x \pm iS^y \quad (2.3)$$

and Holstein-Primakoff transformation [18] (assuming s is the total spin on the site)

$$S^+ = \sqrt{2s} \left(1 - \frac{\beta^\dagger \beta}{2s} \right)^{1/2} \beta \approx \sqrt{2s} \beta, \quad (2.4a)$$

$$S^- = \sqrt{2s} \beta^\dagger \left(1 - \frac{\beta^\dagger \beta}{2s} \right)^{1/2} \approx \sqrt{2s} \beta^\dagger, \quad (2.4b)$$

$$S^z = s - \beta^\dagger \beta \quad (2.4c)$$

we write the Heisenberg Hamiltonian (2.2)

$$\mathcal{H}_1 = J_0 s (\beta_i \beta_j^\dagger + \beta_j^\dagger \beta_i + s - \beta_i^\dagger \beta_i - \beta_j^\dagger \beta_j). \quad (2.5)$$

Here we have neglected terms of order β^4 and higher. The operators β_i^\dagger and β_i are spin deviation creation and annihilation operators, respectively. They satisfy the commutation relations:

$$[\beta_i, \beta_j^\dagger] = \delta_{ij}, \quad (2.6a)$$

$$[\beta_i, \beta_j] = [\beta_i^\dagger, \beta_j^\dagger] = 0. \quad (2.6b)$$

Response of the material (change of magnetisation ΔM) to the field H given by

$$\Delta M(t) = \int_{-\infty}^{+\infty} \frac{d\omega}{2\pi} \varphi_{MM}(\omega) H(\omega) e^{i\omega t}, \quad (2.7)$$

with the response function φ_{MM} satisfying

$$\varphi_{BA}(t) = i\theta(t-\tau) \langle [B(t), A(\tau)] \rangle, \quad (2.8)$$

where $\langle \dots \rangle$ indicates that one should average over a grand canonical ensemble and $\theta(t-\tau)$ denotes the Heaviside step function [19]. Furthermore, we arbitrarily set $\tau = 0$.

We consider the field H causing a time dependent Zeeman perturbation Hamiltonian

$$\delta \mathcal{H} = -\gamma \sum_i \mathbf{S}_i \cdot \mathbf{H}_0 F(t), \quad (2.9)$$

where i sums over all lattice points and dimensionless $F(t)$ assumes all time dependency of field $H(t)$ with amplitude H_0 . The symbol γ denotes the gyromagnetic ratio.

For $\varphi_{M^+ M^-}$ (superscripts referring to the direction of response and field, respectively) a shorter notation is used: φ_{+-} . As the order β^4 was neglected in (2.5), no infinite series of functions is encountered during analysis and so the response functions are exact [19]. Hence the response functions in the frequency-momentum representation are

$$\varphi_{++}(\omega, \mathbf{k}) = \varphi_{--}(\omega, \mathbf{k}) = 0, \quad (2.10a)$$

$$\varphi_{+-}(\omega, \mathbf{k}) = \frac{2s\gamma^2}{A} \frac{1}{\omega + 2J_0 s Z(\gamma_k - 1)}, \quad (2.10b)$$

$$\varphi_{-+}(\omega, \mathbf{k}) = -\frac{2s\gamma^2}{A} \frac{1}{\omega - 2J_0 s Z(\gamma_k - 1)}, \quad (2.10c)$$

where A is the area of the structure, Z is the number of next nearest carbon neighbours in the structure and

$$\gamma_k = \frac{1}{Z} \sum_{\delta} e^{-i\mathbf{k} \cdot \delta} \quad (2.11)$$

with δ as the lattice vector between next nearest-neighbours.

Due to linear behaviour of the response function in linear response theory, spin relations (2.3) can be used to express the response function (2.10) in x - y direction:

$$\begin{aligned} \varphi_{xx}(\omega, \mathbf{k}) &= \varphi_{yy}(\omega, \mathbf{k}) = \\ &= \frac{1}{4} \left(\frac{2s\gamma^2}{A} \frac{1}{\omega + 2J_0 s Z(\gamma_k - 1)} - \right. \\ &\quad \left. - \frac{2s\gamma^2}{A} \frac{1}{\omega - 2J_0 s Z(\gamma_k - 1)} \right), \end{aligned} \quad (2.12a)$$

$$\begin{aligned} \varphi_{xy}(\omega, \mathbf{k}) = -\varphi_{yx}(\omega, \mathbf{k}) = \\ = \frac{i}{4} \left(\frac{2s\gamma^2}{A} \frac{1}{\omega + 2J_0 s Z (\gamma_k - 1)} + \right. \\ \left. + \frac{2s\gamma^2}{A} \frac{1}{\omega - 2J_0 s Z (\gamma_k - 1)} \right). \end{aligned} \quad (2.12a)$$

We consider a pulse with carrier frequency Ω lasting for duration of 2τ acting on the graphene system in the x -direction:

$$H^x(t) = H_0 e^{i\Omega t} (\theta(t+\tau) - \theta(t-\tau)). \quad (2.13)$$

In frequency space, this signal can be expressed as

$$H^x(\omega) = \frac{2H_0 \sin((\omega - \Omega)\tau)}{\omega - \Omega}. \quad (2.14)$$

Hence the response of the system in x -direction to the signal (2.13) is given by (2.7) with the response function (2.12a)

$$\begin{aligned} \Delta M^x(t) = \frac{s\gamma^2}{2} \int \frac{d^2 k}{(2\pi)^2} \int \frac{d\omega}{2\pi} \gamma_k H^x(\omega) e^{i\omega t} \times \\ \times \left(\frac{1}{\omega + \omega_k - i\varepsilon} + \frac{1}{\omega - \omega_k - i\varepsilon} \right), \end{aligned} \quad (2.15)$$

where

$$\omega_k = 2J_0 s Z (\gamma_k - 1), \quad (2.16)$$

and $\varepsilon \rightarrow 0$ is a small parameter shifting the poles of response function away from the integration path which includes the x -axis.

Integration over frequency domain can be performed analytically using the residue theorem and Jordan's lemma. During the duration of the signal ($t < \tau$), the response becomes

$$\begin{aligned} \Delta M^x(t) = M_0 \int \frac{d^2 k}{(2\pi)^2} \gamma_k \times \\ \times \left(\frac{e^{i\Omega t} - e^{-i\omega_k t} \cos((\omega_k + \Omega)\tau)}{\omega_k + \Omega} + \right. \\ \left. + \frac{e^{i\Omega t} - e^{-i\omega_k t} \cos((\omega_k - \Omega)\tau)}{\omega_k - \Omega} \right), \end{aligned} \quad (2.17a)$$

however when the signal is no longer active (for times $t > \tau$), the response is given by

$$\begin{aligned} \Delta M^x(t) = iM_0 \int \frac{d^2 k}{(2\pi)^2} \gamma_k \times \\ \times \left(\frac{e^{-i\omega_k t} \sin(\omega_k + \Omega)\tau}{\omega_k + \Omega} - \right. \\ \left. - \frac{e^{-i\omega_k t} \sin(\omega_k - \Omega)\tau}{\omega_k - \Omega} \right), \end{aligned} \quad (2.17b)$$

where $M_0 = s\gamma^2 H_0 / 2$.

3. Dispersion relation

The un-hydrogenated carbon in triangular graphene has $Z = 6$ next nearest-neighbours which are in the vertices of the hexagon units (see Fig. 1). Direct evaluation of (2.11) gives γ_k :

$$\gamma_k = \frac{1}{3} \cos \sqrt{3} k_y a_0 + \frac{2}{3} \cos \frac{3}{2} k_x a_0 \cos \frac{\sqrt{3}}{2} k_y a_0, \quad (3.1)$$

and (2.16) gives the energy:

$$\begin{aligned} \omega_k = \pm \omega_0 \left(1 - \frac{1}{3} \cos \sqrt{3} k_y a_0 - \right. \\ \left. - \frac{2}{3} \cos \frac{3}{2} k_x a_0 \cos \frac{\sqrt{3}}{2} k_y a_0 \right), \end{aligned} \quad (3.2)$$

where $\omega_0 = 2J_0 s Z$. These expressions are then substituted into (2.17).

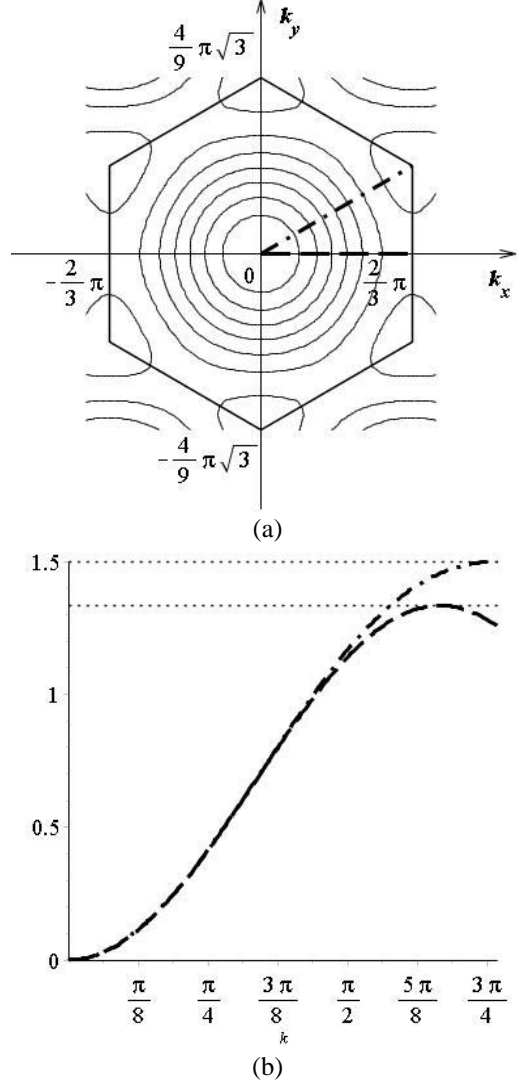


Fig. 3. Spin wave dispersion relation: a) – energy profile contour plot; b) – cross-sections from the Brillouin zone center to the maximum (dash-dotted line) and to the saddle point (dashed line)

The energy surface contour plot and its cross-sections are shown in Fig. 3,a and 3,b, respectively; the hexagonal shape bounds the 1st Brillouin zone. The energy surface has three types of critical points.

The first is a global minimum at the origin, where $\omega_{\vec{k}} = 0$. The energy is proportional to k^2 around the centre, and the dispersion relation is almost isotropic here. Nevertheless, the integrals for magnetisation response or internal energy of spin waves gas diverge making the isotropic approximation inapplicable.

The Brillouin zone perimeter includes 6 maxima where $\omega_{\vec{k}} = 3\omega_0/2$ and 6 saddle points with $\omega_{\vec{k}} = 4\omega_0/3$. We will show below that these characteristic points are responsible for the resonance behaviour of the spin waves in graphene.

4. Numerical method

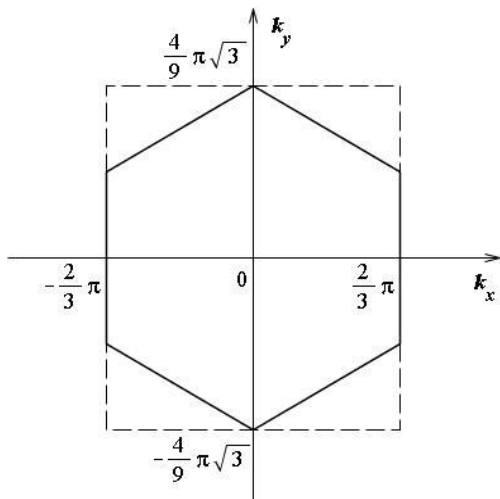


Fig. 4. The 1st Brillouin zone (solid line) and rectangular integration area (dashed line)

The transversal magnetisation given by (2.16) is evaluated numerically. Integration with respect to wave-vector is provided within the 1st Brillouin zone (Fig. 4). The applied method uses a uniform Cartesian grid in the rectangle and checks whether current wave-vector \vec{k} is within the hexagon:

$$\Delta M(t_q) \approx \frac{1}{(2\pi)^2} \sum_{i,j} f(k_{x,i}, k_{y,j}, t_q) (\Delta k)^2, \quad (4.1)$$

where Δk is the grid step in momentum space - equal for both x and y directions, $f(k_{x,i}, k_{y,j}, t_q)$ is the integrand in (2.16), and t_q is the discretised time. Calculated magnetisation is normalized to the maximum of its absolute value.

The grid has 100 nodes along k_x -axis. Test calculations with 50 and 200 nodes show that the integration is converged.

Fourier spectrum of magnetisation signal is evaluated from the previously calculated data. It is realized

by approximation of continuous Fourier transform by numerical integration with respect to the time:

$$\Delta M(\omega) \approx \sum_q \Delta M(t_q) e^{-i\omega q} \Delta t, \quad (4.2)$$

where Δt is the time discretisation step.

The algorithms are executed in FORTRAN-90 language with OpenMP parallelization over independent variable t and ω , respectively.

5. Magnetisation response

The magnetisation response to a transversal pulse of a duration τ is evaluated for different Ω . The pulse excites oscillations of magnetisation, which decay after it ends. Characteristic decay time strongly depends on carrier frequency. There are three main signal types (based on carrier frequency) which can be considered.

The first occurs when $\Omega < 4\omega_0/3$ (we refer this as a “low-frequency” pulse). The dynamics of the positive envelope of M_x for $\Omega = \omega_0$ is shown in Fig. 5,a, and its Fourier spectrum is visualised in Fig. 5,b. The magnetisation signal is normalized to its maximum value. This interval does not contain any characteristic frequency of spin waves. Therefore the magnetisation decays fast with characteristic time near $30\omega_0^{-1}$. The Fourier spectrum shows oscillations in the whole interval of possible spin wave frequencies with sharp peak at $3\omega_0/2$. These oscillations are induced by the edges of the pulse.

The second type of dynamics occurs when $\Omega > 3\omega_0/2$ (referred to as “high-frequency”). Here, the magnetisation oscillates weakly with frequency Ω during the pulse, and large-amplitude signal is caused by the falling edge of the pulse (Fig. 6,a). After the pulse, the magnetisation oscillates with frequency close to the dispersion relation maximum $\omega_{\vec{k}} = 3\omega_0/2$, therefore two peaks occur in spectrum (Fig. 6,b). The characteristic decay time is the same as in the previous case.

The pulse with carrier frequency in the interval $4\omega_0/3 < \Omega < 3\omega_0/2$ (“near resonance” pulse) may produce a resonance excitation of spin waves when Ω is close to the frequency corresponding to the critical points of dispersion relation (see Fig. 3). In this case, the transversal magnetisation decays slowly during the time $\sim (100 \div 150)\omega_0^{-1}$ (Fig. 7, a). At this frequency, the Fourier spectrum contains only one dominant peak (Fig. 7, b).

Carrier frequency between the critical points ($\Omega = 7\omega_0/5$) produces relatively weak response during the pulse and the beating with the period is close to $30\omega_0^{-1}$ after the pulse; the beat pattern amplitude also decays over a long period of time. The spectrum of such signal also contains one bright peak. Its fine structure cannot be resolved in Fig. 7, b.

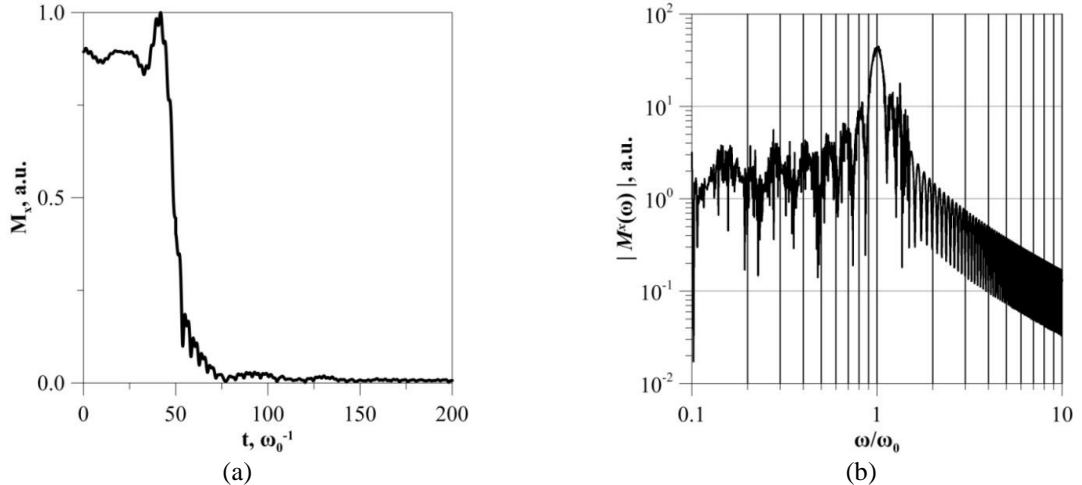


Fig. 5. Response of triangular graphene on low frequency pulse, $\Omega = \omega_0$ a) – transversal magnetisation envelope; b) – Fourier spectrum of the signal

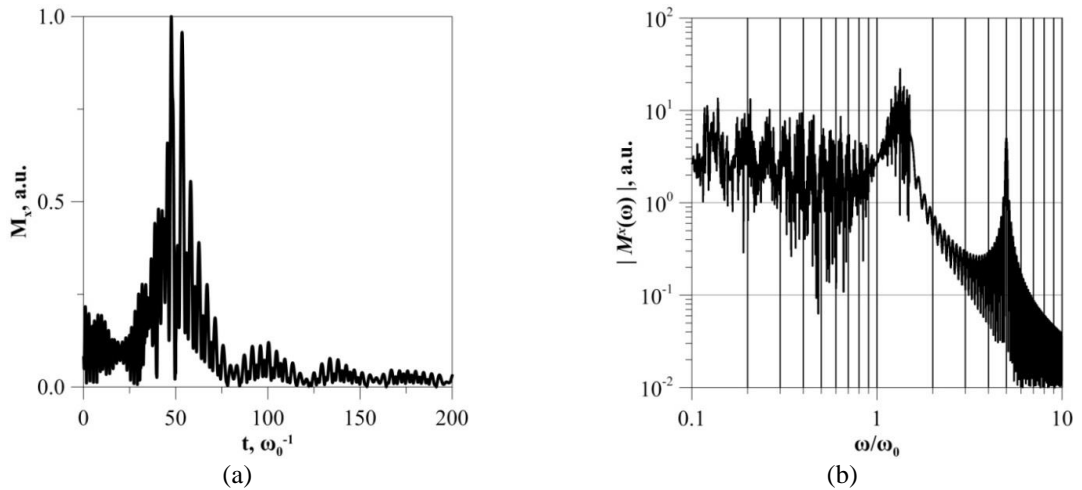


Fig. 6. Response of triangular graphene on high frequency pulse, $\Omega = 5\omega_0$: a) – transversal magnetisation envelope; b) – Fourier spectrum of the signal

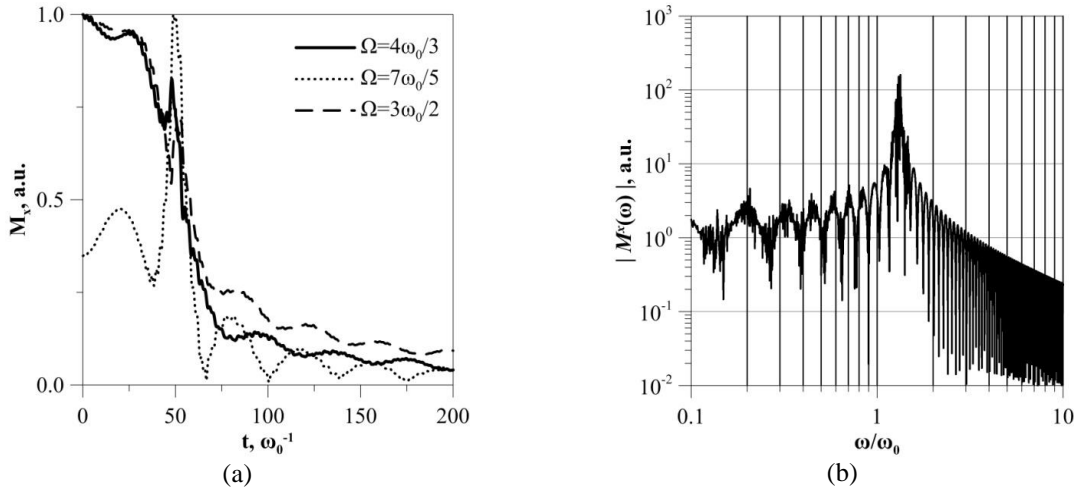


Fig. 7. Response of triangular graphene on ‘near resonance’ pulse: a) – transversal magnetisation envelope, $\Omega = 4\omega_0/3$ (solid lines), $\Omega = 7\omega_0/5$ (dotted lines), $\Omega = 3\omega_0/2$ (dashed lines); b) – Fourier spectrum of the signal, $\Omega = 4\omega_0/3$

6. Conclusion

The results demonstrate a possible way for experimental measurement of the exchange energy J_0 be-

tween un-hydrogenated carbons in graphone as it determines the characteristic frequencies in the magnetisation spectra (see (2.16) and (3.2)).

There are few known papers evaluating J_0 using density functional theory [20, 21]. In these studies, the

obtained exchange value varies from -1 meV [20] to -33 meV when the spin-spin interaction is fully-screened by Coulomb repulsion of the conduction electrons, and to -98 meV if there is no screening [21]. The first estimate corresponds to frequency around $1.5 \cdot 10^{12}$ Hz; the two latter values give the frequency in interval from $4.8 \cdot 10^{13}$ Hz to $1.4 \cdot 10^{14}$ Hz. The characteristic decay time for “near resonance” pulse is of the order 10^{-10} s in the former case, and 10^{-12} s in the latter.

This suggests that THz or far-infrared spectroscopy could be used to measure the exchange energy parameter. Our results show the resonance will be at frequencies which correspond to the upper limit of spin wave energy band ($\Omega = 3\omega_0/2$) and the saddle points of energy surface ($\Omega = 4\omega_0/3$).

The exchange value also determines the applicability of the spin waves approach for the description of magnetisation. If the coefficient is of the order 1 meV, the spin waves will be suppressed by thermal fluctuations at temperatures greater than 10 K. Larger values of the exchange energy extend the domain of spin wave existence to 380 K with interaction screening and to 1100 K without it. These temperatures are much larger than the thermal limit of graphene stability estimated in literature [13].

We are grateful for the financial support of the scholarship provided by the British Petroleum and the University of Oxford’s Career Service Office which enabled us to get these scientific results. K. Tsiberkin is also thankful to Russian Foundation for Basic Research, Grant N. 17-42-590271.

Список литературы

1. Castro Neto A.H., Guinea F., Peres N. M. R., Novoselov K. S., Geim A. K. The electronic properties of graphene // *Reviews of Modern Physics*. 2009. Vol. 81, 109. DOI: 10.1103/RevModPhys.81.109
2. Geim A. K., Novoselov K. S. The rise of graphene // *Nature Materials*. 2007. Vol. 6. P. 183–191. DOI: 10.1038/nmat1849
3. Geim A. K. Graphene: status and prospects // *Science*. 2009. Vol. 324, N. 5934. P. 1530–1534. DOI: 10.1126/science.1158877
4. Saremi S. RKKY in half-filled bipartite lattice: graphene as an example // *Physical Review B*. 2007. Vol. 76, 184430. DOI: 10.1103/PhysRevB.76.184430
5. Britnell L., Gorbachev R. V., Jalil R. et al. Field-effect tunneling transistor based on vertical graphene heterostructures // *Science*. 2012. Vol. 335, N. 6071. P. 947–950. DOI: 10.1126/science.1218461
6. Sorella S., Tosatti E. Semi-metal-insulator transition of the Hubbard model in the honeycomb lattice // *Europhysics Letters*. 1992. Vol. 19. N. 8, P. 699–704. DOI: 10.1209/0295-5075/19/8/007
7. Hemmatyan S., Polini M., Abanov A. et al. Stable path to ferromagnetic hydrogenated graphene // *Physical Review B*. 2014. Vol. 90, 035433. DOI: 10.1103/PhysRevB.90.035433
8. Boukhvalov D. W., Katsnelson M. I. Chemical functionalization of graphene // *Journal of Physics: Condensed Matter*. 2009. Vol. 21, 344205. DOI: 10.1088/0953-8984/21/34/344205
9. Brar V. W., Decker R., Solowan H. et al. Gate-controlled ionization and screening of cobalt adatoms on a graphene surface // *Nature Physics*. 2011. Vol. 7. P. 43–47. DOI: 10.1038/NPHYS1807
10. Eelbo T., Waśniowska M., Gyamfi M. et al. Influence of the degree of decoupling of graphene on the properties of transition metal adatoms // *Physical Review B*. 2013. Vol. 87, 205443. DOI: 10.1103/PhysRevB.87.205443
11. Kogan E. RKKY interaction in gapped or doped graphene // *Graphene*. 2013. Vol. 2, N. 1. P. 8–12. DOI: 10.4236/graphene.2013.21002
12. Zhou J., Wang Q., Sun Q., Chen X. S., Kawazoe Y., Jena P. Ferromagnetism in semihydrogenated graphene sheet // *Nano Letters*. 2009. Vol. 9, N. 11. P. 3867–3870. DOI: 10.1021/nl9020733
13. Подливаев А. И., Опенов Л. А. О термической устойчивости графона // *Физика и техника полупроводников*. 2011. Т. 45, № 7. С. 988–991.
14. Feng L., Zhang W. X. The structure and magnetism of graphene // *AIP Advances*. 2012. Vol. 2, 042138. DOI: 10.1063/1.4766937
15. Kharche N., Nayak S. K. Quasiparticle band gap engineering of graphene and graphone on hexagonal boron nitride substrate // *Nano Letters*. 2011. Vol. 11, N. 12. P. 5274–5278. DOI: 10.1021/nl202725w
16. Boukhvalov D. W. Stable antiferromagnetic graphone // *Physica E*. 2010. Vol. 43. P. 199–201. DOI: 10.1016/j.physe.2010.07.015
17. Deacon R. S., Chuang K.-C., Nicholas R. J. et al. Cyclotron resonance study of the electron and hole velocity in graphene monolayers // *Physical Review B*. 2007. Vol. 76, 081406. DOI: 10.1103/PhysRevB.76.081406
18. Holstein T., Primakoff H. Field dependence of the intrinsic domain magnetization of a ferromagnet // *Physical Review*. 1940. Vol. 58, 1098. DOI: 10.1103/PhysRev.58.1098
19. Зубарев Д. Н. Двухвременные функции Грина в статистической физике // *Успехи физических наук*. 1960. Т. 71. С. 71–116. DOI: 10.3367/UFNr.0071.196005c.0071
20. Rudenko A. N., Keil F. J., Katsnelson M. I., Lichtenstein A. I. Exchange interactions and frustrated magnetism in single-side hydrogenated and fluorinated graphene // *Physical Review B*. 2013. Vol. 88, 081405(R). DOI: 10.1103/PhysRevB.88.081405

21. Masurenko V. V., Rudenko A. N., Nikolaev S. A., Medvedeva D. S., Lichtenstein A. I., Katsnelson M. I. Role of direct exchange and Dzyaloshinskii–Moriya interactions in magnetic properties of graphene derivatives: C₂F and C₂H // *Physical Review B*. 2016. Vol. 94, 214411. DOI: 10.1103/PhysRevB.94.214411 DOI: 10.1103/PhysRevB.87.205443
11. Kogan E. RKKY interaction in gapped or doped graphene. *Graphene*, 2013, vol. 2, no. 1, pp. 8–12. DOI: 10.4236/graphene.2013.21002
12. Zhou J., Wang Q., Sun Q., Chen X. S., Kawazoe Y., Jena P. Ferromagnetism in semihydrogenated graphene sheet *Nano Letters*, 2009, vol. 9, no. 11, pp. 3867–3870. DOI: 10.1021/nl9020733
13. Podlivaev A. I., Openov L. A. On the thermal stability of graphene. *Semiconductors*, 2011, vol. 45, no. 7, pp. 958–961. DOI: 10.1134/S1063782611070177
14. Feng L., Zhang W. X. The structure and magnetism of graphene. *AIP Advances*, 2012, vol. 2, 042138. DOI: 10.1063/1.4766937
15. Kharche N., Nayak S. K. Quasiparticle band gap engineering of graphene and graphane on hexagonal boron nitride substrate. *Nano Letters*, 2011, vol. 11, no. 12, pp. 5274–5278. DOI: 10.1021/nl202725w
16. Boukhvalov D. W. Stable antiferromagnetic graphene. *Physica E*, 2010, vol. 43, pp. 199–201. DOI: 10.1016/j.physe.2010.07.015
17. Deacon R. S., Chuang K.-C., Nicholas R. J. et al. Cyclotron resonance study of the electron and hole velocity in graphene monolayers. *Physical Review B*, 2007, vol. 76, 081406. DOI: 10.1103/PhysRevB.76.081406
18. Holstein T., Primakoff H. Field dependence of the intrinsic domain magnetization of a ferromagnet. *Physical Review*, 1940, vol. 58, no. 1098. DOI: 10.1103/PhysRev.58.1098
19. Zubarev D. N. Double-time Green functions in statistical physics. *Soviet Physics Uspekhi*, 1960, vol. 3, pp. 320–345. DOI: 10.1070/PU1960v003n03ABEH003275
20. Rudenko A. N., Keil F. J., Katsnelson M. I., Lichtenstein A. I. Exchange interactions and frustrated magnetism in single-side hydrogenated and fluorinated graphene. *Physical Review B*, 2013, vol. 88, 081405(R). DOI: 10.1103/PhysRevB.88.081405
21. Masurenko V. V., Rudenko A. N., Nikolaev S. A., Medvedeva D. S., Lichtenstein A. I., Katsnelson M. I. Role of direct exchange and Dzyaloshinskii–Moriya interactions in magnetic properties of graphene derivatives: C₂F and C₂H. *Physical Review B*, 2016, vol. 94, 214411. DOI: 10.1103/PhysRevB.94.214411.

Просьба ссылаться на эту статью в русскоязычных источниках следующим образом:

Циберкин К. Б., Гажи М. Магнитный отклик треугольного графона // Вестник Пермского университета. Физика. 2018. № 3 (41). С. 65–72. doi: 10.17072/1994-3598-2018-3-65-72

Please cite this article in English as:

Tsberkin K. B., Gaži M. Magnetic response of triangular graphene // Bulletin of Perm University. Physics, 2018, no. 3 (41), pp. 65–72. doi: 10.17072/1994-3598-2018-3-65-72